Available online at www.sciencedirect.com
SCIENCE DIRECT
Physics Letters B 638 (2006) 450–454
PHYSICS LETTERS B
www.elsevier.com/locate/physletb

Measurement of the analyzing power A_N in pp elastic scattering in the CNI region with a polarized atomic hydrogen gas jet target

H. Okada [e,f], I.G. Alekseev [d], A. Bravar [a,*], G. Bunce [a,b], S. Dhawan [i], R. Gill [a], W. Haeberli [g], O. Jinnouchi [b,1], A. Khodinov [g], Y. Makdisi [a], A. Nass [a,2], N. Saito [e,f], E.J. Stephenson [c], D.N. Svirida [d], T. Wise [h], A. Zelenski [a]

[a] *Brookhaven National Laboratory, Upton, NY 11973, USA*
[b] *RIKEN BNL Research Center, Upton, NY 11973, USA*
[c] *Indiana University Cyclotron Facility, Bloomington, IN 47408, USA*
[d] *Institute for Theoretical and Experimental Physics, 117259 Moscow, Russia*
[e] *Kyoto University, Sakyo-ku, Kyoto 606-8502, Japan*
[f] *RIKEN, Wako, Saitama 351-0198, Japan*
[g] *Stony Brook University, Stony Brook, NY 11794, USA*
[h] *University of Wisconsin, Madison, WI 53706, USA*
[i] *Yale University, New Haven, CT 06520, USA*

Received 13 April 2006; received in revised form 5 June 2006; accepted 6 June 2006

Available online 13 June 2006

Editor: W. Haxton

Abstract

A precise measurement of the analyzing power A_N in proton–proton elastic scattering in the region of 4-momentum transfer squared $0.001 < |t| < 0.032$ $(\mathrm{GeV}/c)^2$ has been performed using a polarized atomic hydrogen gas jet target and the 100 GeV/c RHIC proton beam. The interference of the electromagnetic spin-flip amplitude with a hadronic spin-nonflip amplitude is predicted to generate a significant A_N of 4–5%, peaking at $-t \simeq 0.003$ $(\mathrm{GeV}/c)^2$. This kinematic region is known as the Coulomb nuclear interference region. A possible hadronic spin-flip amplitude modifies this calculable prediction. We present the first precise result of the CNI asymmetry and shape as a function of t. Our data are well described by the CNI prediction with the electromagnetic spin-flip alone and do not support the presence of a large hadronic spin-flip amplitude.

PACS: 13.88.+e; 13.85.Dz; 29.25.Pj

Keywords: Elastic scattering; Spin; Coulomb nuclear interference; Hadronic spin-flip

1. Introduction

Interference phenomena in hadron collisions have often led to spectacular spin effects in the final state. This, for instance, occurs in the elastic scattering of transversely polarized protons at small angles, where the interference of a small spin-flip amplitude, that otherwise would be difficult to detect, with a large spin-nonflip amplitude leads to a sizeable analyzing power A_N. The region of low 4-momentum transfer squared t is associated with long distance phenomena and therefore is in the domain of nonperturbative QCD. Polarized experiments in this region allow us to explore the spin properties of QCD at large distances. A_N is a measure of the *left–right* asymmetry of the cross section in the scattering plane normal to the beam or target polarization.

In high energy pp and pA elastic scattering at very low t, the dominant contribution to A_N comes from the interference between the electromagnetic (Coulomb) spin-flip amplitude, which is generated by the proton's anomalous magnetic

* Corresponding author.
E-mail address: bravar@bnl.gov (A. Bravar).
[1] Present address: KEK, Tsukuba, Ibaraki 305, Japan.
[2] Present address: University of Erlangen, Nurenberg, 91058 Erlangen, Germany.

0370-2693
doi:10.1016/j.physletb.2006.06.008

moment, and the hadronic (nuclear) spin-nonflip amplitudes, which can be related to the total cross section $\sigma_{\rm tot}$ via the optical theorem (thus Coulomb nuclear interference). The CNI asymmetry was first predicted by Schwinger in 1946 [1]. A_N reaches a predicted maximum value of about 4–5% around $-t \simeq 3 \times 10^{-3}(\mathrm{GeV}/c)^2$ and decreases with increasing $|t|$ [2,3]. In general, the form of A_N and the position of its maximum depend on the parameters describing the hadronic amplitudes: $\sigma_{\rm tot}$, the ratio ρ between the real and imaginary parts of the forward scattering amplitude, the Bethe phase shift δ_C, and the nuclear slope parameter b [4].

Several authors (see for instance [4] and references therein) anticipated the existence of hadronic spin-flip amplitudes. The presence of a hadronic spin-flip amplitude interfering with the electromagnetic spin-nonflip one introduces a deviation in shape and magnitude for A_N calculated with no hadronic spin-flip. A measurement of A_N in the CNI region, therefore, can be a sensitive probe for the hadronic spin-flip amplitude. This effect is measured by the ratio r_5 between the single spin-flip ($\phi_5^{\rm had}$) and the spin-nonflip ($\phi_1^{\rm had}$, $\phi_3^{\rm had}$) hadronic amplitudes:

$$r_5 = \lim_{|t|\to 0} \frac{M_p}{\sqrt{-t}} \frac{\phi_5^{\rm had}}{\mathrm{Im}(\phi_1^{\rm had} + \phi_3^{\rm had})/2}, \tag{1}$$

where M_p is the proton mass. In the simplest hypothesis the reduced spin-flip amplitude $\phi_5^{\rm had}/\sqrt{-t}$ is assumed to be proportional to $\phi_1^{\rm had}$ and $\phi_1^{\rm had} = \phi_3^{\rm had}$ [4]. The t dependence of the hadronic spin-flip amplitude, however, is tightly connected with the structure of hadrons at large distances and carries information on the static properties and on the constituent quark structure of the nucleon [5].

Within Regge phenomenology, one can probe the long standing issue of the magnitude of the pomeron spin-flip [4,6]. In a diquark enhanced picture of the proton, for instance, the magnitude of the hadronic spin-flip amplitude is associated with the diquark separation, the smaller this separation the bigger the effect [6]. In the impact model based on the rotating matter picture for a polarized proton the spin-orbit coupling provides a helicity-flip amplitude [7]. Hadronic spin-flip contributions may also have their origins in instantons [8].

A first measurement of A_N at $\sqrt{s} = 19.4$ GeV, though much less precise, had been performed by the E704 experiment at Fermilab using the 200 GeV/c polarized proton beam obtained from the decay of Λ hyperons [9]. Recently, A_N has been measured also at $\sqrt{s} = 200$ GeV by colliding the RHIC polarized proton beams [10].

In this Letter we report on a precise measurement of the analyzing power A_N in the CNI region of $0.001 < |t| < 0.032$ $(\mathrm{GeV}/c)^2$ at $\sqrt{s} = 13.7$ GeV using an internal polarized atomic hydrogen gas jet target and the 100 GeV/c RHIC proton beam. The RHIC collider accelerates transversely polarized protons in bunches of opposite polarization [11]. By averaging over the bunch polarizations and several accelerator fills, one obtains an unpolarized proton beam. The residual beam polarization was less than 1% of the original one.

2. Experimental set-up

Fig. 1 shows the schematic layout of this experiment, located at the 12 o'clock interaction point of RHIC. The polarized atomic hydrogen beam crossed the RHIC proton beams from above. The two RHIC beams were radially displaced by about 10 mm, so that only the beam circulating clockwise interacted with the jet target. The polarization of the atomic beam was directed vertically. In the CNI region at high energies recoil protons from pp elastic scattering emerge close to 90° with respect to the incident beam direction. The scattered beam protons did not exit the beam pipe and were not detected. In the covered t region, however, the elastic process is fully constrained by the recoil particle alone.

The polarized hydrogen jet is produced by an atomic beam source in which molecular hydrogen is dissociated by a radio frequency (RF) discharge. Hydrogen atoms emerge through a 2 mm diameter nozzle cooled to 70 K and enter a set of sextupole magnets that spin separate and focus the atomic beam according to the electron spin. Nuclear polarization of the atoms is obtained using two RF transitions that induce spin-flips in the hydrogen atoms. To avoid depolarization of the atoms a set of Helmholtz coils around the interaction point provided a very uniform vertical magnetic holding field (0.12 T).

The target polarization P_T was constantly monitored with a Breit–Rabi polarimeter located below the interaction point. The net proton polarization was 0.958 ± 0.001. A measured $(3.5 \pm 2.0)\%$ contamination of the atomic beam by hydrogen atoms bound into molecules resulted in a small dilution of the target polarization. Taking into account this dilution, the target polarization P_T was 0.924 ± 0.018. The proton polarization was reversed every 600 s by turning on one or the other of two RF coils. The efficiency of the spin-flip transitions was above 99%. Most systematic effects associated with the spin-asymmetry extraction thus cancel. The atomic jet achieved a polarized beam intensity of 1.2×10^{17} H atoms/s at a speed of (1560 ± 50) m/s, which is the highest intensity recorded to date. At the interaction point the target profile is nearly Gaussian with a FWHM of 6.5 mm. The areal density of the target is $(1.3 \pm 0.2) \times 10^{12}$ H/cm^2. For more details see [12].

The recoil protons were detected using an array of silicon detectors located to the left and to the right of the beam at a

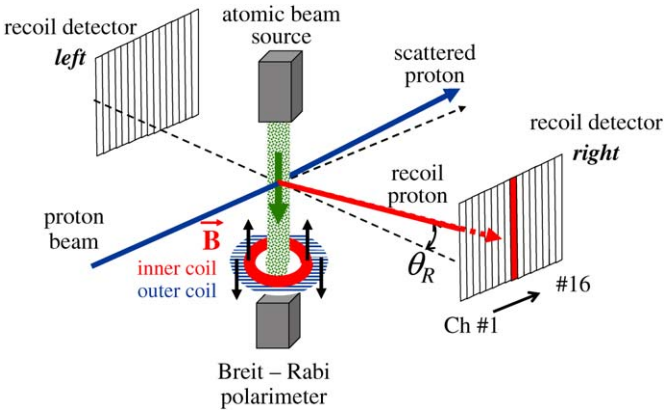

Fig. 1. Schematic layout of this experiment.

distance $D \simeq 80$ cm. On each side, the detectors cover an azimuthal angle of 15° centered on the horizontal mid-plane. Since the momenta of the recoil protons are very low, a second set of Helmholtz coils, coaxial to the first one with the current circulating in the opposite direction, was used to cancel the deflection of the recoil proton trajectory induced by the inner coils. The resulting total magnetic field integral $\int B\,dl$ seen by the recoil protons is nearly zero, and the deviation from the original trajectory was less than 3 mm for the lowest momentum detected protons, leading to an almost identical acceptance for the left and right detectors.

Each array consisted of 3 silicon detectors segmented horizontally, 80×50 mm^2 in size, with a 4.4 mm read out pitch for a total of 16 channels per detector. The detectors were ~ 400 μm thick. Recoil protons with kinetic energies T_R up to 7 MeV were fully absorbed. More energetic protons punched through the detectors, depositing only a fraction of their energy. The energy calibration of the silicon detectors was performed using two α sources of different energies (^{148}Gd and ^{241}Am), which allowed us also to estimate the thickness of the detector's entrance window (~ 2 μm) and correct for it. The detectors were read out with waveform digitizers (WFD) that performed simultanously the function of peak sensing ADC's and constant fraction discriminators, and provided a deadtime free data acquisition system.

The recoil detectors provided energy (T_R), recoil polar angle (ϑ_R), and time of flight (ToF) measurements for the recoil particles. The 4-momentum transfer squared is given by $-t = 2M_p T_R$. The ToF is measured with respect to the bunch crossing given by the accelerator RF clock. Typical resolutions were $\Delta T_R \leqslant 60$ keV, $\Delta\vartheta_R \simeq 3.8$ mrad, and $\Delta\text{ToF} \simeq 3$ ns. The angular resolution receives contributions from the spatial resolution of the detector ($\simeq 1.6$ mrad) and the jet target profile. The ToF resolution comes from the intrinsic time resolution of the detectors ($\leqslant 2$ ns) and the length of the RHIC beam bunches ($\sigma \simeq 1.5$ ns).

3. Elastic scattering events

Recoil protons were identified using the nonrelativistic relation $T_R = \frac{1}{2}M_p(D/\text{ToF})^2$ shown in Fig. 2. Recoil protons of given T_R could be clearly separated from prompt particles on the ToF basis. Below 7 MeV recoil protons are fully absorbed in the detectors. Above 7 MeV, T_R is corrected for punch-through using the detector thickness and the energy loss in silicon [13]. Events were selected in a ToF interval of ±8 ns around the expected ToF value for recoil protons of a given T_R.

pp elastic scattering events are identified on the basis of the ϑ_R–T_R relation $T_R \simeq 2M_p\vartheta_R^2$. Fig. 3 shows the measured E_R–ϑ_R correlation for ToF selected events. In the scatter plot ϑ_R is measured by the detector channel number in $\simeq 5.5$ mrad steps. E_R is the energy deposited by the recoil protons in the detectors. The locus on the left in Fig. 3 is generated by fully absorbed protons, while the locus on the right is due to punch through protons. The full line is the kinematic expectation for pp elastic scattering for fully absorbed protons. The dashed line shows the expected energy deposited in the detector by more energetic protons for $T_R > 7$ MeV.

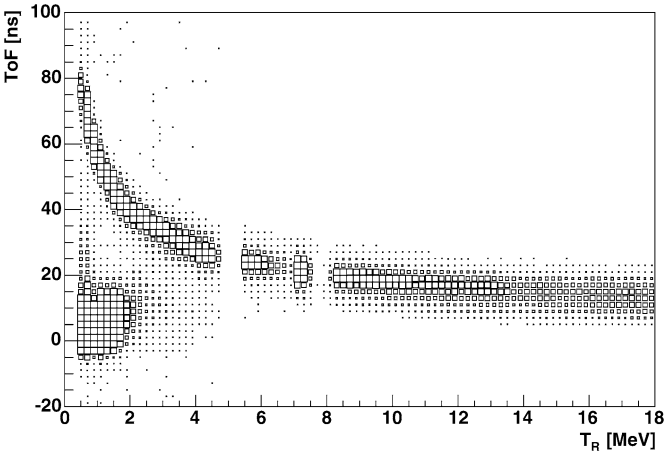

Fig. 2. ToF vs. T_R scatter plot for all recorded events. The locus is populated by recoil protons, while the bulk of events on the bottom left is due to prompt and beam halo events. The *empty* vertical bands are populated by the calibration α sources and have been removed from the plot.

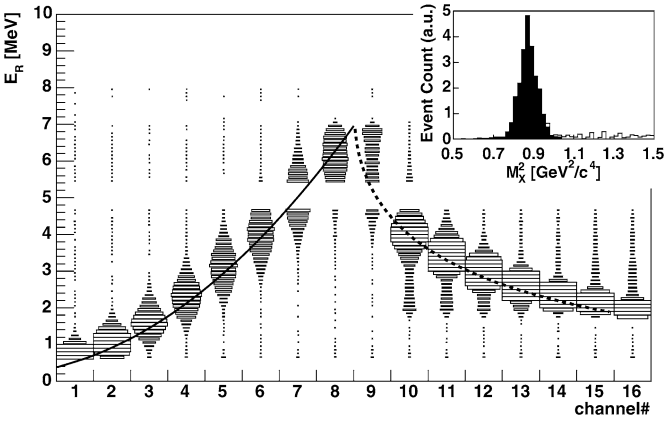

Fig. 3. E_R vs. ϑ_R correlation: ϑ_R is measured by the detector channel number in $\simeq 5.5$ mrad steps. The inset shows the missing mass squared M_X^2. For $1 \leqslant T_R \leqslant 3$ MeV.

For each T_R bin (see Table 1) pp elastic events were selected in 3 adjacent detector channels centered around the expected ϑ_R angle. On the basis of the measured ϑ_R and T_R the mass of the undetected scattered beam particle (the missing mass M_X) can be reconstructed. For pp elastic scattering $M_X = M_p$. The channel for diffractive dissociation opens at $M_X > M_p + M_\pi = 1.08$ GeV/c^2. The selected pp elastic events are well separated from the inelastic threshold for $T_R < 8$ MeV (see inset). The contamination from inelastic channels for larger T_R was estimated to be less than 0.5%.

4. Analyzing power extraction

A_N was extracted from the geometrical mean of spin sorted event yields [14]:

$$A_N = -\frac{1}{P_T}\frac{\sqrt{N_L^{\uparrow}\cdot N_R^{\downarrow}} - \sqrt{N_R^{\uparrow}\cdot N_L^{\downarrow}}}{\sqrt{N_L^{\uparrow}\cdot N_R^{\downarrow}} + \sqrt{N_R^{\uparrow}\cdot N_L^{\downarrow}}}, \tag{2}$$

Table 1
A_N as a function of t in 14 T_R bins. The first error is the statistical one, followed by the systematic error, and the normalization error on P_T

T_R (MeV)	$-\langle t\rangle$ (GeV$^2/c^2$)	A_N	δA_N (stat. $\pm$ sys. $\pm$ norm.)
0.6–1.0	0.0015	0.0348	$0.0017 \pm 0.0030 \pm 0.0007$
1.0–1.4	0.0022	0.0422	$0.0020 \pm 0.0007 \pm 0.0008$
1.4–1.8	0.0030	0.0493	$0.0022 \pm 0.0010 \pm 0.0010$
1.8–2.2	0.0037	0.0442	$0.0023 \pm 0.0006 \pm 0.0009$
2.2–2.5	0.0044	0.0430	$0.0027 \pm 0.0004 \pm 0.0008$
3.0–3.5	0.0061	0.0423	$0.0025 \pm 0.0017 \pm 0.0008$
3.5–4.2	0.0071	0.0363	$0.0021 \pm 0.0018 \pm 0.0007$
4.2–4.7	0.0084	0.0388	$0.0020 \pm 0.0023 \pm 0.0008$
5.7–7.2	0.0118	0.0348	$0.0015 \pm 0.0031 \pm 0.0007$
8.0–9.3	0.0165	0.0272	$0.0023 \pm 0.0016 \pm 0.0005$
9.3–10.6	0.0187	0.0242	$0.0020 \pm 0.0013 \pm 0.0005$
10.6–12.0	0.0212	0.0227	$0.0020 \pm 0.0008 \pm 0.0004$
14.5–16.0	0.0287	0.0271	$0.0021 \pm 0.0018 \pm 0.0005$
16.0–17.0	0.0309	0.0263	$0.0027 \pm 0.0065 \pm 0.0005$

where $N_{L(R)}^{\uparrow(\downarrow)}$ is the number of selected pp elastic scattering events detected on the left(right) of the beam, P_T is the target polarization discussed before, and the arrows give the direction of the target polarization. In this expression flux factors, acceptances, and efficiencies factor out and appear only as third order corrections. Data were gathered in 14 T_R bins (see Table 1).

The level of background under the signal was estimated from empty target runs with and without beam, and sidebands in the strip distributions for fixed recoil energy bins. These backgrounds were flat. The background included α source background, beam scraping, and beam scattering from residual target gas. The overall background level was dependent on the T_R bin: it increased from 6% to 9% for the lowest T_R bins (0.6 to 7.2 MeV) and $\simeq 10\%$ for the punch-through bins (8.0 to 17.0 MeV).

The systematic uncertainties in the measurement are in two categories: T_R bin-dependent and overall normalization. The final A_N values were corrected for α source background and beam gas scattering, determined from empty target runs. The background originating from the unpolarized residual target gas and the target tails has been already accounted for as a dilution of the target polarization. The major sources of systematic uncertainties come from (1) the error on the target polarization giving an overall 2.0% normalization uncertainty, (2) the false and acceptance asymmetries (ranging between 0.0001 and 0.0031 for all T_R bins, except for last T_R bin where they were 0.0064), (3) event selection criteria (between 0.0002 and 0.0018), and (4) the background (between 0.0001 and 0.0003). The background uncertainty from the residual target gas is included in the target polarization uncertainty, which is from two independent measurements. The residual beam polarization, which was consistent with zero, had no effect on this result.

5. Result and conclusion

Fig. 4 displays the analyzing power A_N as a function of t in the range $0.001 < |t| < 0.032(\text{GeV}/c)^2$ at $\sqrt{s} = 13.7$ GeV. These data are summarized in Table 1.

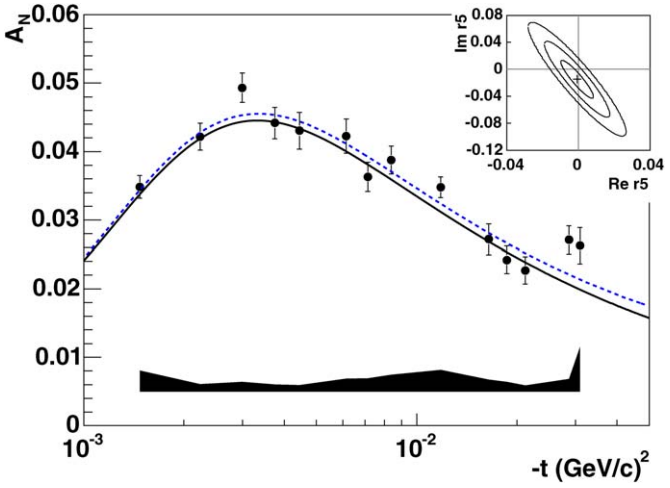

Fig. 4. A_N as a function of t for $pp^{\uparrow} \to pp$ at $\sqrt{s} = 13.7$ GeV. The errors on the data points are statistical. The lower band represents the total systematic error. The prediction for A_N with the electromagnetic spin-flip only is superimposed to the data (solid lane). The dashed line is a fit to the data allowing for a hadronic spin-flip contribution to A_N. Inset: r_5 with the 1-, 2-, and 3-σ confidence contours.

The A_N data are compared to the CNI prediction with no hadronic spin-flip [4] using for the hadronic amplitudes $\sigma_{\text{tot}} = 38.4$ mb, $\rho = -0.08$, $\delta_C = 0.02$, $b = 12(\text{GeV}/c)^{-2}$ [15]. The major uncertainty in the CNI prediction comes from the parametrization of the hadronic amplitudes and the approximate knowledge of the ρ parameter. The χ^2 is 13.4 for 14 degrees of freedom.

The A_N data were also fitted with the CNI prediction allowing for a hadronic spin-flip contribution (Eq. (1), dashed line in Fig. 4). The explicit expression for A_N including the hadronic spin-flip amplitudes (r_5) is given in [4], Eqs. (27)–(29). The quality of the fit is similar to the case with no hadronic spin-flip ($\chi^2 = 11.1/12$ d.o.f.). The values obtained for r_5 are $\text{Re}\, r_5 = -0.0008 \pm 0.0091$ and $\text{Im}\, r_5 = -0.015 \pm 0.029$, and the correlation parameter between $\text{Re}\, r_5$ and $\text{Im}\, r_5$ is -0.92. The results of the r_5 fit are shown as inset in Fig. 4.

These data are consistent with no hadronic spin-flip and do not support the presence of a large hadronic spin-flip amplitude at this energy. A_N data from proton–carbon elastic scattering over a similar kinematic range at the same [16] and lower [17] energies, on the contrary, deviate substantially from the simple CNI prediction and require a substantial hadronic spin-flip contribution.

Finally, this measurement represents the first precise confirmation of the predicted dependence of the analyzing power on the 4-momentum transfer squared t in pp elastic scattering, due to the proton's anomalous magnetic moment of Schwinger [1], Kopeliovich, and Lapidus [2].

Acknowledgements

We thank the Collider Accelerator Department and the RHIC/AGS Operation Groups. We thank the Instrumentation Division at BNL for their work on the silicon detectors and electronics. This work is performed under the auspices of

US DOE contract Nos. DE-AC02-98CH10886 and W-31-109-ENG-38, DOE grant No. DE-FG02-88ER40438, NSF grant PHY-0100348, and with support from RIKEN, Japan.

References

[1] J. Schwinger, Phys. Rev. 69 (1946) 681.
[2] B.Z. Kopeliovich, L.I. Lapidus, Sov. J. Nucl. Phys. 19 (1974) 114.
[3] N.H. Buttimore, E. Gotsman, E. Leader, Phys. Rev. D 18 (1978) 694.
[4] N.H. Buttimore, et al., Phys. Rev. D 59 (1999) 114010.
[5] E. Predazzi, O.V. Selyugin, Eur. Phys. J. A 13 (2002) 471;
A.F. Martin, E. Predazzi, Phys. Rev. D 66 (2002) 034029.
[6] B.Z. Kopeliovich, B.G. Zakharov, Phys. Lett. B 226 (1989) 156.
[7] C. Bourelly, J. Soffer, T.T. Wu, Phys. Rev. D 19 (1979) 3249;
C. Bourelly, J. Soffer, T.T. Wu, Nucl. Phys. B 247 (1984) 15.
[8] M. Anselmino, S. Forte, Phys. Rev. Lett. 71 (1993) 223.
[9] N. Akchurin, et al., Phys. Rev. D 48 (1993) 3026.
[10] S. Bültmann, et al., Phys. Lett. B 632 (2006) 167.
[11] I. Alekseev, et al., Nucl. Instrum. Methods A 499 (2003) 392.
[12] A. Zelenski, et al., Nucl. Instrum. Methods A 536 (2005) 248;
T. Wise, et al., Nucl. Instrum. Methods A 559 (2006) 1.
[13] M.J. Berger, et al., NIST database http://physics.nist.gov/PhysRefData/Star/Text.
[14] G.G. Ohlsen, P.W. Keaton, Nucl. Instum. Methods 109 (1973) 41.
[15] M.M. Block, R.N. Cahn, Rev. Mod. Phys. 57 (1985) 563.
[16] O. Jinnouchi, et al., in: Proceedings of the 16th International Spin Physics Symposium SPIN2004, p. 515.
[17] J. Tojo, et al., Phys. Rev. Lett. 89 (2002) 052302.